Landscapes of polyphase glaciation: eastern Hellas Planitia, Mars

Stephen BROUGH[a*], Bryn HUBBARD[a], Colin SOUNESS[a], Peter M. GRINDROD[b,c] and Joel DAVIS[b,d]

[a]*Department of Geography and Earth Sciences, Aberystwyth University, Aberystwyth, UK*

[b]*Centre for Planetary Sciences, University College London/Birkbeck, London, UK*

[c]*Department of Earth and Planetary Sciences, Birkbeck, University of London, London, UK*

[d]*Department of Earth Sciences, University College London, London, UK*

* Corresponding author. Email: stb20@aber.ac.uk

Contact details:

Stephen Brough: Department of Geography and Earth Sciences, Aberystwyth University, Llandinam Building, Penglais Campus, Aberystwyth, SY23 3DB. 01970 621859. Stb20@aber.ac.uk

Prof Bryn Hubbard: Department of Geography and Earth Sciences, Aberystwyth University, Llandinam Building, Penglais Campus, Aberystwyth, SY23 3DB. 01970 622783. byh@aber.ac.uk

Dr Colin Souness: Department of Geography and Earth Sciences, Aberystwyth University, Llandinam Building, Penglais Campus, Aberystwyth, SY23 3DB. 01970 621859. colinsouness8@googlemail.com

Dr Peter Grindrod: Department of Earth and Planetary Sciences, Birkbeck, University of London, Malet Street, London, WC1E 7HX. 020 7679 7986. p.grindrod@ucl.ac.uk

Joel Davis: Department of Earth Sciences, UCL, Gower Street, London, WC1E 6BT. 020 7679 2577. joel.davis.09@ucl.ac.uk

Abstract: The mid-latitudes of Mars host numerous ice related landforms that bear many similarities to terrestrial ice masses. This collection of landforms, termed viscous flow features (VFFs), are composed primarily of H_2O ice and show evidence of viscous deformation. Recent work has hypothesised that VFFs are the diminishing remains of once larger ice masses, formed during one or more previous ice ages, and the landscape therefore records evidence of polyphase glaciation. However, debate persists concerning the former extent and volume of ice, and style of former glaciations. The accompanying map (1:100,000 scale) presents a geomorphic and structural assessment of a glacial landscape in eastern Hellas Planitia, Mars. Here we present a description of the features identified, comprising four geomorphic units (plains, lobate debris apron, degraded glacial material, and glacier-like form) and 16 structures (craters, moraine-like ridges, flow unit boundary, arcuate transvers structures, longitudinal surface structures, ring-mold craters, terraces, medial-moraine like ridges, raised textured areas, flow-parallel and flow-transverse lineations, crevasses and crevasse traces, and ridge cluster).

Keywords: Mars; ice; glaciation; lobate; debris apron; glacier-like form; mid-latitude; climate change

1. Introduction

The mid-latitudes of Mars host numerous ice related landforms with many similarities to terrestrial ice masses (e.g. Arfstrom and Hartmann, 2005; Head *et al*., 2005; Baker *et al*., 2010; Hubbard *et al*., 2011; Souness *et al*., 2012; Sinha and Murty, 2013). These landforms are composed primarily of H_2O ice, have surface morphologies consistent with viscous deformation and have consequently become known as viscous flow features, or VFFs (Milliken et al., 2003; Holt *et al*., 2008; Plaut *et al*., 2009). Recent advances in orbital and climatic modelling have supported earlier arguments that VFFs are related to geologically-recent ice ages. These ice ages are proposed to occur as a consequence of increased solar radiation forcing water stored in the polar caps of Mars to be transported towards lower latitudes, under periods of high (>30^{o}) obliquity (Touma and Wisdom, 1993; Head *et al*., 2003; Laskar *et al*., 2004; Forget *et al*., 2006).

Despite an increase in research into such non-polar ice deposits on Mars during recent decades, several fundamental planetary and glaciological issues remain, of which our collective understanding is still only in its infancy (see Souness and Hubbard, 2012; Hubbard *et al*., 2014). Of particular prominence is the origin and subsequent evolution of mid-latitude VFFs (e.g. Pierce and Crown, 2003; Parsons *et al*., 2011; Fastook *et al*., 2011, Souness *et al*., 2012; Souness and Hubbard, 2013).

Such VFFs are comprised of four distinct subtypes (see review of Souness and Hubbard, 2012): (i) glacier-like forms, or GLFs (Hartmann, 2003; Hubbard *et al*., 2011); (ii) lobate debris aprons, or LDAs (Squyres, 1978; Pierce and Crown, 2003); (iii) lineated valley fill, or LVF (Squyres, 1978); and (iv) concentric crater fill, or CCF (Levy *et al*., 2010). However, VFFs commonly coalesce and interact to form what Head *et al*. (2010) described as Mars' integrated glacial landsystem (Figure 1). Following this model, GLFs represent the lowest-order component of this glacial landsystem, generally forming in small valleys or cirque-like alcoves. Often multiple GLFs forming adjacent escarpments converge to form broad, rampart-like LDAs. In turn, LDAs may converge or coalesce to form an often complex and contorted surface termed LVF.

[Insert Figure 1 near here]

At present there is a growing body of evidence suggesting that mid-latitude ice deposits are the remnants of a once far larger ice mass (e.g. Dickson *et al*., 2008, 2010; Sinha and Murty, 2013; Hubbard *et al*., 2014) and the widespread identification of glacial features and landforms has led to suggestions that continental scale glaciation may have occurred on Mars (e.g. Kargel *et al*., 1995; Fastook *et al*., 2014). Reconstructing glacial environments based on their landforms and structural assemblage is a powerful concept applied in terrestrial glaciology (see Hubbard and Glasser, 2005). Through utilising evidence left on the landscape with observations from modern glaciers, we can reconstruct the extent and dynamics of both former (glaciated) and modern (glacierised) glacial environments (e.g. Kleman *et al*., 1997; Evans and Twigg, 2002; Greeenwood and Clark, 2009).

The map described herein documents the geomorphic units and structural features associated with a glacial landscape in eastern Hellas Planitia, Mars. Here, we present an overview of the data and methods used, and provide a description of the main units recorded on the map, which can be found as supplementary content to this article.

2. Study site and brief review of previous work

2.1 Study site

Located to the east of Hellas Planitia, one of the largest impact structures on Mars, Reull Vallis is a morphologically complex outflow channel system, which is comprised of Noachian (~4.65-3.7 Ga BP), Hesperian (~3.7-3.0 Ga BP), and Amazonian (~3.0 Ga BP to present) materials (Tanaka and Leonard, 1995; Mest and Crown, 2001). Reull Vallis has an abundant population of VFFs (e.g.; Souness *et al*., 2012), in particular LDAs, of which over 90 have been identified here (Mest and Crown, 2001; Pierce and Crown, 2003). Here, we map a particularly well-developed LDA and associated landforms which surround an isolated highland massif (Figure 2). The massif sits just to the north of the Reull Vallis outflow channel and is centred on ~103^{o} E, 40.6^{o} S. The study site covers an area of 2,647 km^2 to the west of the massif and topography ranges between ~2700 m to -650 m (relative to Mars datum). The LDA extends radially up to ~26 km from the base of the massif and has a maximum and minimum elevation of ~40 m and -610 m respectively, giving an overall elevation difference of ~650 m. Although not investigated, the eastern portion of the massif also contains several ice related landforms (Figure 2c). The appearance of these landforms share several similarities with features described herein, and elsewhere on Mars (e.g. Whalley and Azizi, 2003), and likely reflect a wider cold climate landsystem in Reull Vallis.

[Insert Figure 2 near here]

2.2 Previous work

Eastern Hellas Planitia is a key region in martian climate and glaciological studies. Climatic simulations have revealed the region to have experienced snow accumulation when Mars' obliquity exceeded 45^{o} (Forget *et al*., 2006). Radar data from Mars Reconnaissance Orbiters' (MRO) Shallow Radar (SHARAD) has augmented these findings by detecting massive H_2O ice deposits, buried beneath thin (<10 m) debris layers surrounding LDAs near Reull Vallis (Holt *et al*., 2008). Furthermore, analysis of craters and stratigraphic relationships of LDAs in the Reull Vallis region indicate that LDAs are Lower Amazonian in age, and are the youngest units in the region (Mest and Crown, 2001; Mest and Crown, 2014).

Investigations using high-resolution imagery have identified several lines of evidence for glacier-like flow in VFFs within eastern Hellas Planitia. Using Mars Express High-Resolution Stereo Camera (HRCS) images, Head *et al*. (2005) described numerous surface textures, including sinuous ridges, irregular depressions and flowlines on the surface of an LDA and within crater deposits. These were hypothesised as being indicative of ice-rich, glacier-like viscous flow. Hubbard *et al*. (2014) recently identified surface fracturing on a GLF in eastern Hellas Planitia. These authors argued that the location and geometry of the surface features are comparable to crevasses common on Earth's glaciers, and as such, are a direct indication of ice flow and brittle deformation.

3. Data, methods and software

3.1 Image sources

We use both Context Camera (CTX – Malin et al., 2007) and High Resolution Imaging Science Experiment (HiRISE – McEwen et al., 2007) imagery, acquired from the Mars Reconnaissance Orbiter (MRO) satellite (Table 1). CTX images have a spatial resolution of ~6 m per pixel and cover an area up to 30 x 160 km (Zurek and Smrekar, 2007). CTX imagery was supplemented by HiRISE imagery where available. HiRISE images have an unparalleled spatial resolution of up to ~0.25 m and cover an area up to 6 x 12 km (Zurek and Smrekar, 2007). For global and regional context, we also use the Mars Orbiter Laser Altimeter (MOLA – Smith et al., 1999) gridded digital terrain model (DTM), with a typical resolution of 460 m per pixel, and the global mosaic of Thermal Emission Imaging System (THEMIS – Edwards et al., 2011) daytime infra-red images, with a typical resolution of 100 m per pixel. All data used in this study are available through the NASA Planetary Data System (PDS).

We created a 20 m per pixel DTM using standard techniques with Integrated Software for Imagers and Spectrometers (ISIS) and SOCET SET ® software packages (Kirk et al., 2008) and the CTX stereo image pair D15_032978_1391_XN_40S257W and D16_033400_1391_XN_40S257W. Using previous methods (Kirk et al., 2003; 2008; Okubo, 2010), we estimate the vertical precision of our CTX stereo DTM to be 3.5 m. We then used this DTM to produce a 6 m per pixel orthorectified image, which was the main data product used in this study.

[Insert Table 1 near here]

3.2 Surface mapping

All mapping and analysis was carried out in ESRI's ArcMap 10.1 Geographical Information System (GIS) software. Mapping was conducted through manual inspection of the imagery. Geomorphic unit and structural classifications were guided by both terrestrial and martian cryospheric literature (e.g. Goodsell *et al*., 2005; Hubbard and Glasser, 2005; Baker *et al*., 2010; Souness and Hubbard, 2013). Standard image enhancement procedures (e.g. histogram equalization, standard deviation) were applied on an image-by-image basis to enhance the appearance and maximise the contrast between features during digitisation.

Features mapped include a lobate debris apron, a glacier-like form, degraded glacial material, crevasses, moraine-like ridges, lineations, terraces, craters, and flow units. Digitisation was carried out at two main scales: (i) 1:50,000 was used for large scale features, including lobate debris apron and plains; and (ii) 1:25,000 was used for less well resolved features such as crevasses, lineations, and moraine-like ridges. Features which varied in size, such as craters and terraces, were mapped at scales appropriate to their characteristics.

4. Description of geomorphic units and structural features

This section describes the geomorphic units and their associated structural features progressing from the distal to proximal end of the glacial system as follows: (i) plains; (ii) LDA; (iii) degraded glacial material; and (iv) GLF. To avoid repetition, although presented in all relevant geomorphic units, a structure will only be described in the first unit where it occurs in the text.

[Insert Figure 3 near here]

4.1 Plains

Plains form the distal part of the glacial landscape, representing an area of ice-free or ice-poor terrain that is texturally distinct from the surrounding ice-related surfaces. The distal plains are characterised by a heavily cratered, but otherwise relatively smooth surface. There is no evidence for surface flow within this unit. Identifying such areas of terrain that appear unaffected by ice flow is important when looking at glacial reconstruction as it provides a clear outer boundary for active glaciation. Structures observed within the plains unit are: (i) craters; and (ii) sinuous ridges.

4.1.1 Craters

Craters are identified as surface depressions caused by the impact of a hypervelocity object – usually a meteoroid (Figure 3a). They are typically bowl-shaped, and quasi circular in planform, but their appearance can change over time. Deformation within the substrate of the material can cause the craters to distort and therefore provide an indication of local strain (e.g. Sinha and Murty, 2013). The appearance or sharpness of craters may also change over time as surface processes degrade their surface terrains and edges (e.g. Baker *et al*., 2010). Craters form an essential part of planetary investigation as they provide a means by which surfaces may be dated (e.g. Hartmann and Neukum, 2001).

4.1.2 Sinuous ridges

Sinuous ridges are identified as ridges that display both positive raised relief from their surroundings and a sinuous morphology (Figure 3a). Ridges may be branched and connect to each other, or occur in isolation. They often interact with craters where they appear to emanate away from, or are dissected by them. These ridges are predominantly located in the northern part of the map. However, one particular prominent sinuous ridge appears to be buried under the upper northern part of the LDA, before emanating into the foreground in a north west direction. It is possible that these ridges are subglacial in origin (i.e. similar to eskers on Earth); however, their morphology is more consistent with 'wrinkle' and degraded ridges in the Reull Valles region, the origin of which are interpreted to be fluvial or volcanic (Mest and Crown, 2001; Mest and Crown, 2014).

4.2 Lobate debris apron (LDA)

Forming the outer ice terrain, the LDA is identified as the region that extends from, and runs parallel to, the base of the massif in a convex down-slope profile, and terminates in a lobate margin. The LDA surface has a relatively rough appearance when compared to the smoother plains material and is heavily textured with a ridge-and-trough pattern, generally aligned transverse to the unit's inferred flow direction. Towards the distal end of the LDA the observed ridge and trough pattern gives way to a more lumpy texture, characterised by small, rounded, butte-like mounds, although this surface type is not ubiquitous across the whole LDA. Identified within the southern part of the LDA, in the foreground of the GLF, is an extensive (~ 90 km^2) area of relatively smooth terrain that contrasts with the surrounding rough LDA texture. Running parallel to the northern part of the LDA are a series of moraine-like ridges, which occur up to ~1 km beyond the current LDA limit. The LDA is the most extensive ice terrain and, based on a qualitative assessment of crater density, also the oldest.

The surface morphology and convexity described above have previously been used to infer that LDAs show viscous flow, and that the mechanism by which flow is achieved is a result of ice deformation (e.g. Squyres, 1978; Colaprete and Jakosky, 1998; Pierce and Crown, 2003; Head *et al*., 2005; Holt *et al*., 2008; Grindrod and Fawcett, 2011). Structures observed within the LDA unit are: (i) moraine-like ridges; (ii) flow unit boundaries; (iii) arcuate transverse structures; (iv) longitudinal surface structures; (v) ring-mold craters; and (vi) craters (Section 4.1.1).

4.2.1 Moraine-like ridges

Moraine-like ridges are long (10^1 km), often narrow (10^{-2} – 10^{-1} km), ridges that are raised above their surroundings (Figure 3b). Moraine-like ridges are identified running parallel to the terminus of VFFs, commonly in an arcuate manner and are similar to terminal or ice-marginal moraines associated with terrestrial glaciers (Arfstrom and Hartmann, 2005). Such moraines (and Mars' moraine-like ridges), mark the former terminal position of an ice mass and are therefore indicators of ice recession, and can also indicate a former boundary between a previously glaciated and currently glacierised terrain. On Earth, moraines form an essential component of glacial reconstruction in both glacierised (e.g. Evans and Twigg, 2002) and glaciated environments (e.g. Greenwood and Clark, 2009).

4.2.2 Flow unit boundaries

A flow unit boundary is identified as a boundary between two flow units that have distinctive velocity fields with an associated discontinuity in orientation of deformation related features (Figure 3c). Structures may also appear smeared along the junction (Goodsell *et al*., 2005).

4.2.3 Arcuate transverse structures

Arcuate transverse structures are identified as linear structures with positive or negative relief that are arranged roughly transverse to the apparent flow direction. These linear structures can be followed down the LDA, where they become highly arcuate or deformed (Figure 3d). Arcuate transverse structures can provide an indication of local flow rates and the distribution of stresses within the flowing material.

4.2.4 Longitudinal surface structures

Longitudinal structures are identified as extended linear features (up to ~20 km long) that are arranged roughly parallel to the apparent flow direction (Figure 3e). These structures are similar in appearance and persistence to longitudinal foliation identified on terrestrial glaciers. However, there is ongoing debate as to the terminology, origin and significance of these features (see Glasser and Gudmundsson, 2012). This debate notwithstanding, both flow transverse and flow parallel (Section 4.2.3) structures can be used to elucidate local flow direction, deformation and strain history (e.g. Baker *et al*., 2010; Souness and Hubbard, 2013).

4.2.5 Ring-mold craters

In contrast to (standard) craters (Section 4.1.1), ring-mold craters are identified as an almost rimless depression with an annular moat enclosing an inner circular plateau of varying morphology (Figure 3f) (e.g. Kress and Head, 2008).The morphology of ring-mold craters is consistent with previous laboratory experiments of impact craters forming in relatively pure ice (e.g. Kato *et al*., 1995), and show a distinctly different morphology to craters formed in ice-poor surfaces. This distinct difference in morphology between ring-mold and bowl shaped craters has led to the interpretation that ring-mold craters are formed in an ice-rich substrate (Kress and Head, 2008). Furthermore, ring-mold craters appear to be exclusively located within VFFs, and therefore have the potential to be a diagnostic indicator for the presence of subsurface ice (Kress and Head, 2008).

4.3 Degraded glacial material

Occupying the base and encroaching up the slopes of the massif is an area of homogeneous terrain characterised by a texturally smoothed surface, abundant terrace structures, and a concave down-slope profile. In contrast to the plains and LDA, there is little evidence of surface cratering on this homogeneous terrain. Several small alcoves appear to be cut into the massif, but two larger alcoves (one located towards the centre of the massif and one on the southern face) are associated with structures, including raised textured areas and moraine-like ridges, similar to the adjacent GLF (Section 4.4). This overall appearance suggests a deflated or degraded terrain, possibly formed during the region's current state of periglaciation. Based on structural evidence within the alcoves, it may also be possible that GLFs once occupied these localities, and therefore localised glaciation may have previously occurred in this unit. Structures observed within this degraded glacial material unit are: (i) terraces; (ii) raised textured area; (iii) medial moraine-like ridges; (iv) moraine-like ridges (Section 4.2.1); and (v) craters (Section 4.1.1).

4.3.1 Terraces

Terraces are identified as an interlinked network of step-like ridges that form sub-perpendicular to slope (Figure 3g). Their length, size and coherence appear highly variable, which correspondingly produces a variety of patterns. Terraces cut across other structures (such as moraine- and medial moraine-like ridges), suggesting that these features represent a later age of formation relative to the structure across which they cut.

4.3.2 Medial moraine-like ridges

Medial moraine-like ridges, in contrast to moraine-like ridges (section 4.2.1), persist longitudinally within an ice mass, rather than forming an arcuate structure demarking a limit of glaciation. Medial moraines are important structures on glaciers on Earth as they can be used to identify flow pathways and the deformation of debris within a glacier (e.g. Hambrey *et al.*, 1999). They are also often flow unit boundaries(section 4.2.2).

4.3.3 Raised textured area

Raised textured areas are identified as areas showing a distinct lumpy surface texture that is raised above the surrounding mass (Figure 3h). The occurrence of a markedly different surface texture to adjacent areas suggests that there is a local change in mechanical process or material composition.

4.4 Glacier-like form (GLF)

A well pronounced GLF with clearly distinguishable outlines occupies a small, cirque-like alcove on the south-western flank of the massif. The GLF has a discernible head and terminus, the latter of which appears to have breached a cirque lip to the northwest of the feature. Running parallel to the terminus of the breached snout is an extensive moraine-like ridge (Section 4.2.1), enclosing the GLF. Within the body of the GLF are several distinct structures indicative of flow and transportation of mass down-slope, including fractures and surface lineations (Hubbard *et al*., 2014). Two large textured areas are identifiable on the lower surface of the GLF, the southernmost of which is associated with a cluster of ridges. Like the degraded glacial material (Section 4.3), the GLF surface has a distinct lack of craters. The GLF appears to reflect a currently glacierised environment, indicative of local ice accumulation and subsequent flow. Structures observed in the GLF unit are: (i) flow-parallel and flow-transverse lineations; (ii) crevasses and crevasse traces; (iii) ridge cluster; (iv) moraine-like ridges (Section 4.2.1); (v) raised textured area (Section 4.3.3); (vi) craters (Section 4.1.1); and (vii) ring-mold craters (Section 4.2.5).

4.4.1 Flow-parallel and flow-transverse lineations

Flow-parallel and flow-transverse lineations show many similarities to the longitudinal and arcuate structures found in the LDA unit (section 4.2) (Figure 3i, j). However, both flow-parallel and flow-transverse lineations only show positive relief and their length is an order of magnitude smaller (up to ~1 km long). Like longitudinal and arcuate surface structures, flow-parallel and flow-traverse lineations can be used to elucidate local flow direction, deformation and strain history (e.g. Baker *et al*., 2010; Souness and Hubbard, 2013).

4.4.2 Crevasse and crevasse trace

Crevasses are identified as an open fracture on the GLF surface and they may cut across other structures (Figure 3k).Crevassing occurs where the tensile strain rate exerted upon and within ice exceeds a temperature-dependant threshold (Vaughan, 1993). Crevasses are correspondingly orientated perpendicular to the direction of maximum extensional strain (Hambrey and Lawson, 2000). Crevasse traces are identified by distinct, often dark, lines in areas of crevassing that do not have a visible opening or fracture. Crevasse traces are former crevasses, which have subsequently closed, likely due to the crevasse passing through a compressive flow regime (Figure 3k) (Hambrey and Lawson, 2000).

4.4.3 Ridge cluster

Identified as a collection of ridges with a sub-parallel, stacked appearance (Figure 3l). Ridges are clustered towards the south west of the GLF where they merge with the raised textured area and are difficult to identify individually. However, individual structures are easily identifiable to the north of the feature, where ridges become well defined.

5. Conclusions

This paper presents a detailed geomorphic and structural map of glacial landforms in eastern Hellas Planitia, Mars. Initial evidence suggest that the region has undergone at least two, possibly three, phases of glaciation, with a wider, more extensive glacial period being recorded in the LDA, and a secondary, more localised glaciation recorded in the GLF. The work presented here is part of a wider ongoing project addressing the extent and dynamics of mid-latitude VFFs on Mars (e.g. Hubbard *et al*., 2014). It also provides further evidence, and extends the spatial scale, for the hypothesis that Mars has experienced multiple phases of glaciation.

Software

Image pre-processing was carried out in the freely-available Integrated Software for Imagers and Spectrometers (ISIS) provided by the United States Geological Survery (USGS). Stereo DTM production was carried out in the commercial software package SOCET SET ® provided by BAE Systems. Image processing and mapping was carried out using ESRI ArcMap 10.1 Geographic Information System (GIS). Figures and final map were produced in ESRI ArcMap 10.1. Figures were subsequently exported to Adobe Illustrator v2.59 for annotation.

Acknowledgements

The authors would like to thank Hannes Bernhardt, John Abrahams and Stephan Harrison for reviewing an earlier version of this manuscript and accompanying map, and both Mike Smith and Monica Pondrelli for editing. The stereo DTM processing was carried out at the UK NASA RPIF at

University College London. SB is funded by an Aberystwyth University Doctoral Career Development Scholarship. PMG is funded by the UK Space Agency (Aurora Fellowship grant ST/L00254X/1).

Map design

The accompanying map was produced with the following: co-ordinate system = GCS Mars; projection = Plate Carree; Datum = Mars; unit = metres; scale = 1:100,000; and paper size A1. The detailed inset map has the same information as above, but has a scale of 1:35,000.

References

Arfstrom, J., & Hartmann, W. K. (2005). Martian flow features, moraine-like ridges, and gullies: Terrestrial analogs and interrelationships. *Icarus, 174*(2), 321-335. doi: 10.1016/j.icarus.2004.05.026

Baker, D. M. H., Head, J. W., & Marchant, D. R. (2010). Flow patterns of lobate debris aprons and lineated valley fill north of Ismeniae Fossae, Mars: Evidence for extensive mid-latitude glaciation in the Late Amazonian. *Icarus, 207*(1), 186-209. doi: 10.1016/j.icarus.2009.11.017

Colaprete, A., & Jakosky, B. M. (1998). Ice flow and rock glaciers on Mars. *Journal of Geophysical Research-Planets, 103*(E3), 5897-5909. doi: 10.1029/97je03371

Dickson, J. L., Head, J. W., & Marchant, D. R. (2008). Late Amazonian glaciation at the dichotomy boundary on Mars: Evidence for glacial thickness maxima and multiple glacial phases. *Geology, 36*(5), 411. doi: 10.1130/g24382a.1

Dickson, J. L., Head, J. W., & Marchant, D. R. (2010). Kilometer-thick ice accumulation and glaciation in the northern mid-latitudes of Mars: Evidence for crater-filling events in the Late Amazonian at the Phlegra Montes. *Earth and Planetary Science Letters, 294*(3-4), 332-342. doi: 10.1016/j.epsl.2009.08.031

Edwards, C. S., Nowicki, K. J., Christensen, P. R., Hill, J., Gorelick, N., & Murray, K. (2011). Mosaicking of global planetary image datasets: 1. Techniques and data processing for Thermal Emission Imaging System (THEMIS) multi-spectral data. *Journal of Geophysical Research: Planets, 116*(E10), E10008. doi: 10.1029/2010je003755

Evans, D. J. A., & Twigg, D. R. (2002). The active temperate glacial landsystem: a model based on Breioamerkurjokull and Fjallsjokull, Iceland. *Quaternary Science Reviews, 21*(20-22), 2143-2177. doi: 10.1016/S0277-3791(02)00019-7

Fastook, J. L., Head, J. W., Forget, F., Madeleine, J.-B., & Marchant, D. R. (2011). Evidence for Amazonian northern mid-latitude regional glacial landsystems on Mars: Glacial flow models using GCM-driven climate results and comparisons to geological observations. *Icarus, 216*(1), 23-39. doi: 10.1016/j.icarus.2011.07.018

Fastook, J. L., Head, J. W., & Marchant, D. R. (2014). Formation of lobate debris aprons on Mars: Assessment of regional ice sheet collapse and debris-cover armoring. *Icarus, 228*, 54-63. doi: 10.1016/j.icarus.2013.09.025

Forget, F., Haberle, R. M., Montmessin, F., Levrard, B., & Head, J. W. (2006). Formation of glaciers on Mars by atmospheric precipitation at high obliquity. *Science, 311*(5759), 368-371. doi: 10.1126/science.1120335

Glasser, N. F., & Gudmundsson, G. H. (2012). Longitudinal surface structures (flowstripes) on Antarctic glaciers. *The Cryosphere, 6*(2), 383-391. doi: 10.5194/tc-6-383-2012

Goodsell, B., Hambrey, M. J., Glasser, N. F., Nienow, P., & Mair, D. (2005). The structural glaciology of a temperate valley glacier: Haut Glacier d'Arolla, Valais, Switzerland. *Arctic Antarctic and Alpine Research, 37*(2), 218-232. doi:10.2307/4139080

Greenwood, S. L., & Clark, C. D. (2009). Reconstructing the last Irish Ice Sheet 1: changing flow geometries and ice flow dynamics deciphered from the glacial landform record. *Quaternary Science Reviews, 28*(27-28), 3085-3100. doi: 10.1016/j.quascirev.2009.09.008

Grindrod, P. M., & Fawcett, S. A. (2011) Possible climate-related signals in high resolution topography of lobate debris aprons in Tempe Terra, Mars. Geophys. Res. Lett., 38, L19201, doi:10.1029/2011GL049295.

Hambrey, M. J., Bennett, M. R., Dowdeswell, J. A., Glasser, N. F., & Huddart, D. (1999). Debris entrainment and transfer in polythermal valley glaciers. *Journal of Glaciology, 45*(149), 69-86

Hambrey, M. J., & Lawson, W. (2000). Structural styles and deformation fields in glaciers: a review. *Geological Society, London, Special Publications, 176*(1), 59-83. doi: 10.1144/gsl.sp.2000.176.01.06

Hartmann, W. (2003). Martian hillside gullies and Icelandic analogs. *Icarus, 162*(2), 259-277. doi: 10.1016/s0019-1035(02)00065-9

Hartmann, W. K., & Neukum, G. (2001). Cratering chronology and the evolution of Mars. *Space Science Reviews, 96*(1-4), 165-194. doi: 10.1023/A:1011945222010

Head, J. W., Marchant, D. R., Dickson, J. L., Kress, A. M., & Baker, D. M. (2010). Northern mid-latitude glaciation in the Late Amazonian period of Mars: Criteria for the recognition of debris-covered glacier and valley glacier landsystem deposits. *Earth and Planetary Science Letters, 294*(3-4), 306-320. doi: 10.1016/j.epsl.2009.06.041

Head, J. W., Mustard, J. F., Kreslavsky, M. A., Milliken, R. E., & Marchant, D. R. (2003). Recent ice ages on Mars. *Nature, 426*(6968), 797-802. doi: 10.1038/Nature02114

Head, J. W., Neukum, G., Jaumann, R., Hiesinger, H., Hauber, E., Carr, M., . . . Team, H. C.-I. (2005). Tropical to mid-latitude snow and ice accumulation, flow and glaciation on Mars. *Nature, 434*(7031), 346-351. doi: 10.1038/Nature03359

Holt, J. W., Safaeinili, A., Plaut, J. J., Head, J. W., Phillips, R. J., Seu, R., . . . Gim, Y. (2008). Radar Sounding Evidence for Buried Glaciers in the Southern Mid-Latitudes of Mars. *Science, 322*(5905), 1235-1238. doi: 10.1126/science.1164246

Hubbard, B., & Glasser, N. F. (2005). *Field Techniques in Glaciology and Glacial Geomorphology*. Chichester: Wiley.

Hubbard, B., Milliken, R. E., Kargel, J. S., Limaye, A., & Souness, C. (2011). Geomorphological characterisation and interpretation of a mid-latitude glacier-like form: Hellas Planitia, Mars. *Icarus, 211*(1), 330-346. doi: 10.1016/j.icarus.2010.10.021

Hubbard, B., Souness, C., & Brough, S. (2014). Glacier-like forms on Mars. *The Cryosphere, 8*(6), 2047-2061. doi: 10.5194/tc-8-2047-2014

Kargel, J. S., Baker, V. R., Beget, J. E., Lockwood, J. F., Pewe, T. L., Shaw, J. S., & Strom, R. G. (1995). Evidence of Ancient Continental-Glaciation in the Martian Northern Plains. *Journal of Geophysical Research-Planets, 100*(E3), 5351-5368. doi: 10.1029/94je02447

Kato, M., Iijima, Y., Arakawa, M., Okimura, Y., Fujimura, A., Maeno, N., & Mizutani, H. (1995). Ice-on-Ice Impact Experiments. *Icarus, 113*(2), 423-441. doi: 10.1006/icar.1995.1032

Kirk, R. L., Howington-Kraus, E., Redding, B., Galuszka, D., Hare, T. M., Archinal, B. A., . . . Barrett, J. M. (2003). High-resolution topomapping of candidate MER landing sites with Mars Orbiter

Camera narrow-angle images. *Journal of Geophysical Research-Planets, 108*(E12). doi: 10.1029/2003je002131

Kirk, R. L., Howington-Kraus, E., Rosiek, M. R., Anderson, J. A., Archinal, B. A., Becker, K. J., . . . McEwen, A. S. (2008). Ultrahigh resolution topographic mapping of Mars with MRO HiRISE stereo images: Meter-scale slopes of candidate Phoenix landing sites. *Journal of Geophysical Research, 113*. doi: 10.1029/2007je003000

Kleman, J., Hattestrand, C., Borgstrom, I., & Stroeven, A. (1997). Fennoscandian palaeoglaciology reconstructed using a glacial geological inversion model. *Journal of Glaciology, 43*(144), 283-299

Kress, A. M., & Head, J. W. (2008). Ring-mold craters in lineated valley fill and lobate debris aprons on Mars: Evidence for subsurface glacial ice. *Geophysical Research Letters, 35*(23). doi: 10.1029/2008gl035501

Laskar, J., Correia, A. C. M., Gastineau, M., Joutel, F., Levrard, B., & Robutel, P. (2004). Long term evolution and chaotic diffusion of the insolation quantities of Mars. *Icarus, 170*(2), 343-364. doi: 10.1016/j.icarus.2004.04.005

Levy, J., Head, J. W., & Marchant, D. R. (2010). Concentric crater fill in the northern mid-latitudes of Mars: Formation processes and relationships to similar landforms of glacial origin. *Icarus, 209*(2), 390-404. doi: 10.1016/j.icarus.2010.03.036

Malin, M. C., Bell, J. F., Cantor, B. A., Caplinger, M. A., Calvin, W. M., Clancy, R. T., . . . Wolff, M. J. (2007). Context Camera Investigation on board the Mars Reconnaissance Orbiter. *Journal of Geophysical Research, 112*(E5). doi: 10.1029/2006je002808

Mest, S. C., & Crown, D. A. (2001). Geology of the Reull Vallis Region, Mars. *Icarus, 153*, 89-110. doi: 10.1006/icar.2001.6655

Mest, S.C., and Crown, D.A. (2014). Geologic map of MTM –30247, –35247, and –40247 quadrangles, Reull Vallis region of Mars. U.S. Geological Survey Scientific Investigations Map *3245,* scale 1:1,000,000, pamphlet 20 p. doi: http://dx.doi.org/10.3133/sim3245

McEwen, A. S., Eliason, E. M., Bergstrom, J. W., Bridges, N. T., Hansen, C. J., Delamere, W. A., . . . Weitz, C. M. (2007). Mars Reconnaissance Orbiter's High Resolution Imaging Science Experiment (HiRISE). *Journal of Geophysical Research, 112*(E5). doi: 10.1029/2005je002605

Milliken, R. E., Mustard, J. F., & Goldsby, D. L. (2003). Viscous flow features on the surface of Mars: Observations from high-resolution Mars Orbiter Camera (MOC) images. *Journal of Geophysical Research, 108*(E6). doi: 10.1029/2002je002005

Okubo, C. H. (2010), Structural geology of Amazonian-aged layered sedimentary deposits in southwest Candor Chasma, Mars, *Icarus*, 207, 210-225, doi:10.1016/j.icarus.2009.11.012.

Parsons, R. A., Nimmo, F., & Miyamoto, H. (2011). Constraints on martian lobate debris apron evolution and rheology from numerical modeling of ice flow. *Icarus, 214*(1), 246-257. doi: 10.1016/j.icarus.2011.04.014

Pierce, T. L., & Crown, D. A. (2003). Morphologic and topographic analyses of debris aprons in the eastern Hellas region, Mars. *Icarus, 163*(1), 46-65. doi: 10.1016/s0019-1035(03)00046-0

Plaut, J. J., Safaeinili, A., Holt, J. W., Phillips, R. J., Head, J. W., Seu, R., . . . Frigeri, A. (2009). Radar evidence for ice in lobate debris aprons in the mid-northern latitudes of Mars. *Geophysical Research Letters, 36*(2), doi: 10.1029/2008gl036379

Sinha, R. K., & Murty, S. V. S. (2013). Evidence of extensive glaciation in Deuteronilus Mensae, Mars: Inferences towards multiple glacial events in the past epochs. *Planetary and Space Science, 86*, 10-32. doi: 10.1016/j.pss.2013.09.002

Smith, D. E., Zuber, M. T., Frey, H. V., Garvin, J. B., Head, J. W., Muhleman, D. O., . . . Sun, X. (2001). Mars Orbiter Laser Altimeter: Experiment summary after the first year of global mapping of Mars. *Journal of Geophysical Research, 106*(E10), 23689. doi: 10.1029/2000je001364

Souness, C., & Hubbard, B. (2012). Mid-latitude glaciation on Mars. *Progress in Physical Geography, 36*(2), 238-261. doi: 10.1177/0309133312436570

Souness, C., Hubbard, B., Milliken, R. E., & Quincey, D. (2012). An inventory and population-scale analysis of martian glacier-like forms. *Icarus, 217*(1), 243-255. doi: 10.1016/j.icarus.2011.10.020

Souness, C. J., & Hubbard, B. (2013). An alternative interpretation of late Amazonian ice flow: Protonilus Mensae, Mars. *Icarus, 225*(1), 495-505. doi: 10.1016/j.icarus.2013.03.030

Squyres, S. W. (1978). Martian Fretted Terrain - Flow of Erosional Debris. *Icarus, 34*(3), 600-613. doi: 10.1016/0019-1035(78)90048-9

Tanaka, K. L., & Leonard, G. J. (1995). Geology and Landscape Evolution of the Hellas Region of Mars. *Journal of Geophysical Research-Planets, 100*(E3), 5407-5432. doi: 10.1029/94je02804

Touma, J., & Wisdom, J. (1993). The Chaotic Obliquity of Mars. *Science, 259*(5099), 1294-1296. doi: 10.1126/science.259.5099.1294

Vaughan, D. G. (1993). Relating the Occurrence of Crevasses to Surface Strain Rates. *Journal of Glaciology, 39*(132), 255-266

Zurek, R. W., & Smrekar, S. E. (2007). An overview of the Mars Reconnaissance Orbiter (MRO) science mission. *Journal of Geophysical Research, 112*(E5). doi: 10.1029/2006je002701

Table 1: List of imagery used in mapping

Instrument	Scene ID	Date (dd/mm/yyyy)	Resolution (m)	Scene Centre	
				Lat. (^{o})	Long. (^{o})
CTX	D15_032978_1391_XN_40S257W	09/08/2013	6	-40.92	102.58
CTX	D16_033400_1391_XN_40S257W	11/09/2013	6	-40.94	102.59
HiRISE	PSP_004272_1390_RED	25/06/2007	0.25	-40.50	102.45
HiRISE	ESP_011669_1390_RED	21/01/2009	0.50	-40.88	102.50
HiRISE	ESP_019462_1390_RED	20/09/2010	0.25	-40.76	102.37
HiRISE	ESP_033400_1390_RED	11/11/2013	0.25	-40.84	102.62
HiRISE	ESP_033901_1390_RED	20/10/2013	0.25	-40.86	102.74
HiRISE	ESP_035391_1390_RED	13/02/2014	0.50	-40.49	102.56

Figure 1: Example of an integrated glacial landsystem as described by Head *et al*., 2010. Each component of the landsystem is labelled as follows: (i) GLFs; (ii) LDAs; (iii) LVFs; and (iv) CCF. The valley floor shows a complex, heavily distorted surface, typical of the integrated glacial landsystem. This scene is a subset of CTX image G02_018857_2226_XI_42N309W (centred 42.62° N, 50.51° E).

Figure 2: Location and expansion of massif studied herein. (a) Global context indicting massifs location to the east of Hellas impact basin, illustrated as a MOLA elevation transparency overlain on a THEMIS-IR day mosaic. (b) Regional context of the Reull Vallis region as seen in THEMIS-IR day mosaic. The region is characterised by large outflow channel systems and abundant montane outcrops. Reull Vallis runs directly below the massif and portions of the Dao, Niger, and Harmakhis Vallis are also identifiable along the western part of the image (orientated NE-SW). (c) CTX mosaic of massif investigated. The LDA can be clearly seen encircling the massif. The area mapped in this study is identified by the red box and represents the DTM extent (section 3.1). Black dots indicate central location of features identified in Figure 3. Mosaic comprised from subset of CTX images D13_03226_1393_XI_40S256W; G16_024552_1394_XI_40S257W; D10_031066_1393_XI_40S257W; and P16_007397_1382_XN_41S257W.

Figure 3: Feature identification in CTX and HiRISE imagery, as discussed in the main text. Images orientated north up. (a) Craters and sinuous ridge. (b) Moraine-like ridge surrounding LDA. (c) Flow unit boundary - arcuate structures can be seen deforming along the flow unit boundary in the centre of the image. (d) Arcuate transverse ridges. (e) Longitudinal surface structure. (f) Well-formed ring-mold crater. (g) Terraces and medial moraine-like ridges – terraces appear to cut across the two medial moraine-like ridges, which run longitudinally from the top centre to bottom centre of the image. (h) Raised textured area – visible on the western and central portion of the image is a lumpy, raised surface texture that clearly contrasts the smoother terrain to the east. (i) Flow-parallel lineations. (j) Flow-transverse lineations. (k) Crevasses (open fracture) and crevasse traces (closed fracture). (l) ridge cluster. Images used: a, c, d, f -ESP_035391_1390_RED; b - PSP_004272_1390_RED; e, g - D15_032978_1391_XN_40S257W orthorectified image (see Section 3.1); and h, I, j, k, l - ESP_033400_1390_RED.

Figure 1.

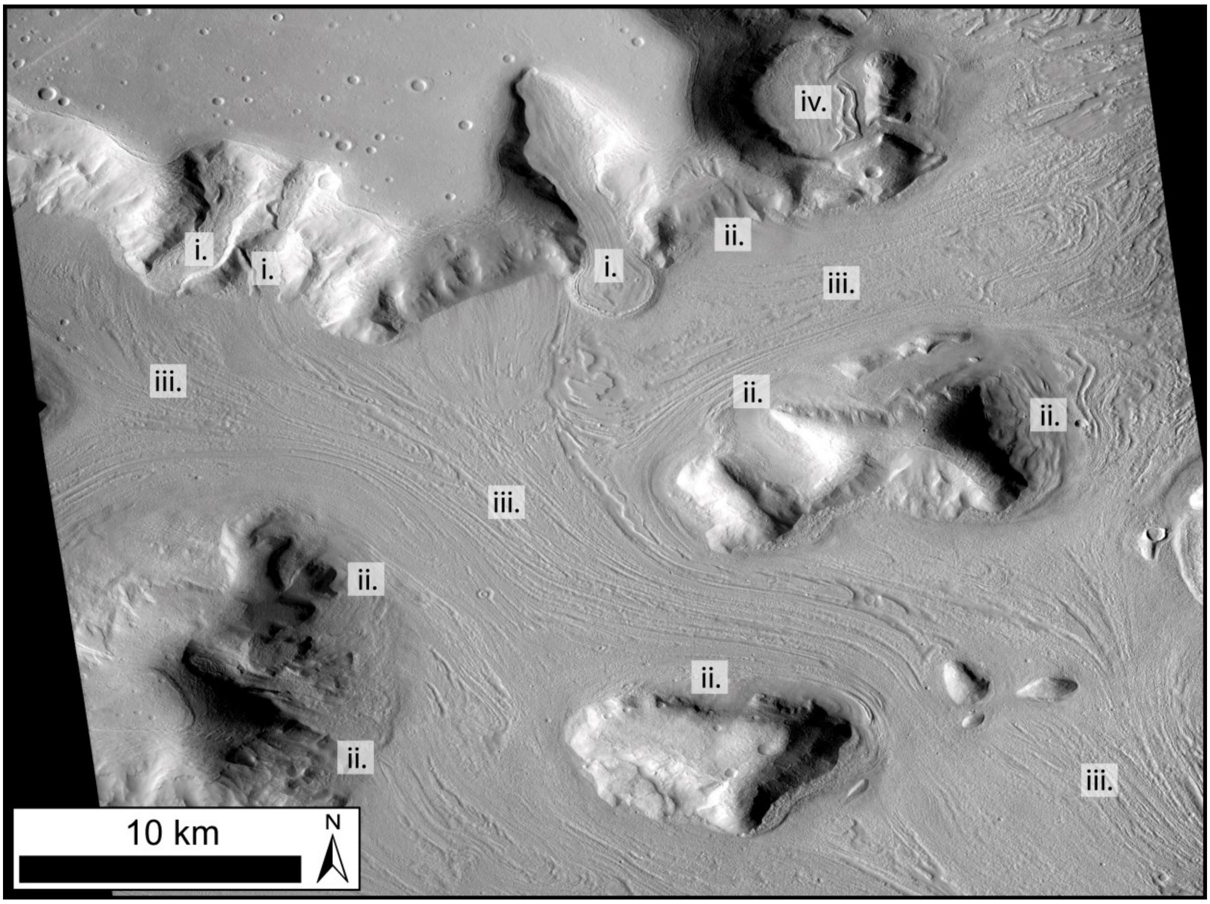

Figure 2.

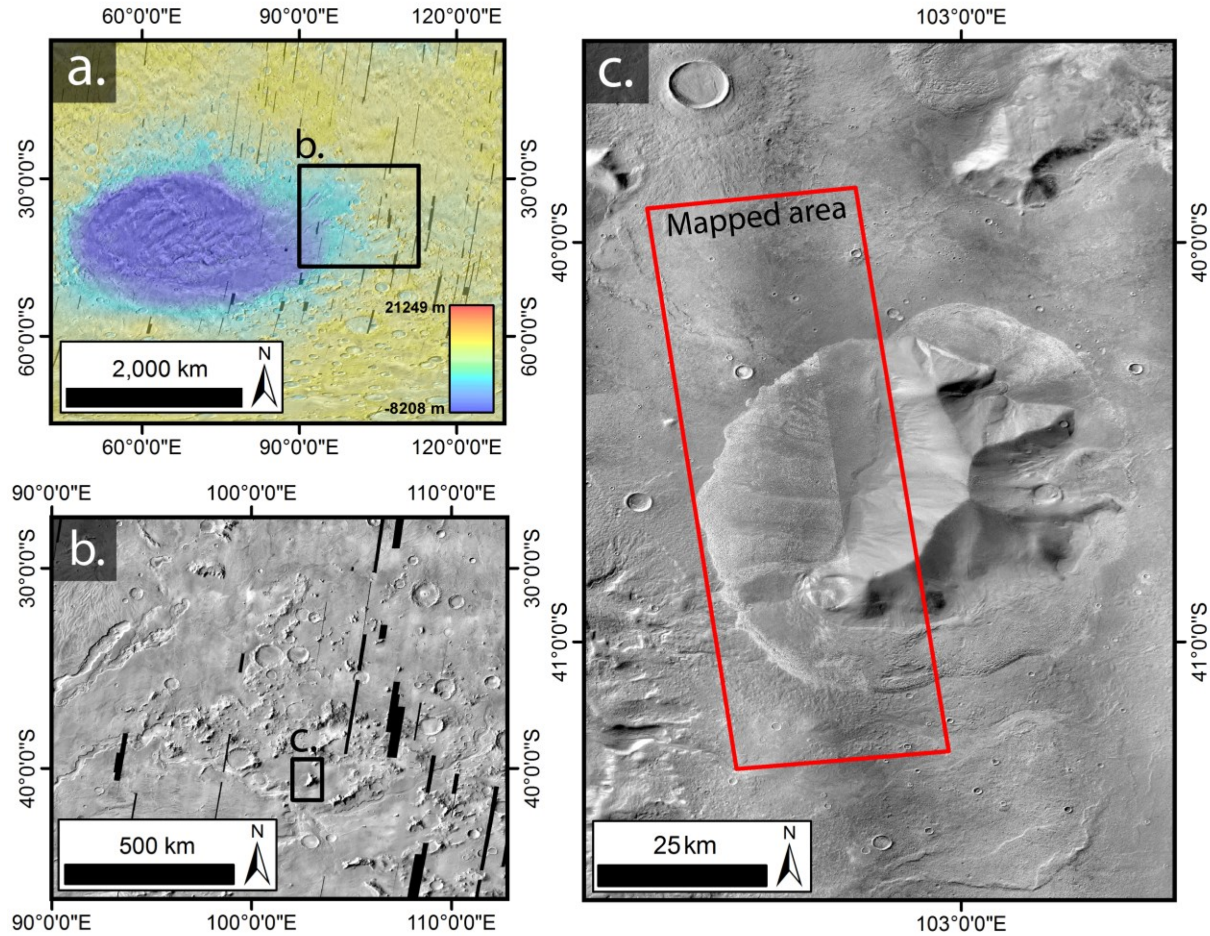

a.
b.
60°0'0"E
90°0'0"E
120°0'0"E
30°0'0"S
60°0'0"S
21249 m
-8208 m
2,000 km
N
b.
c.
90°0'0"E
100°0'0"E
110°0'0"E
30°0'0"S
40°0'0"S
500 km
N
c.
Mapped area
103°0'0"E
40°0'0"S
41°0'0"S
25 km
N

Figure 3.

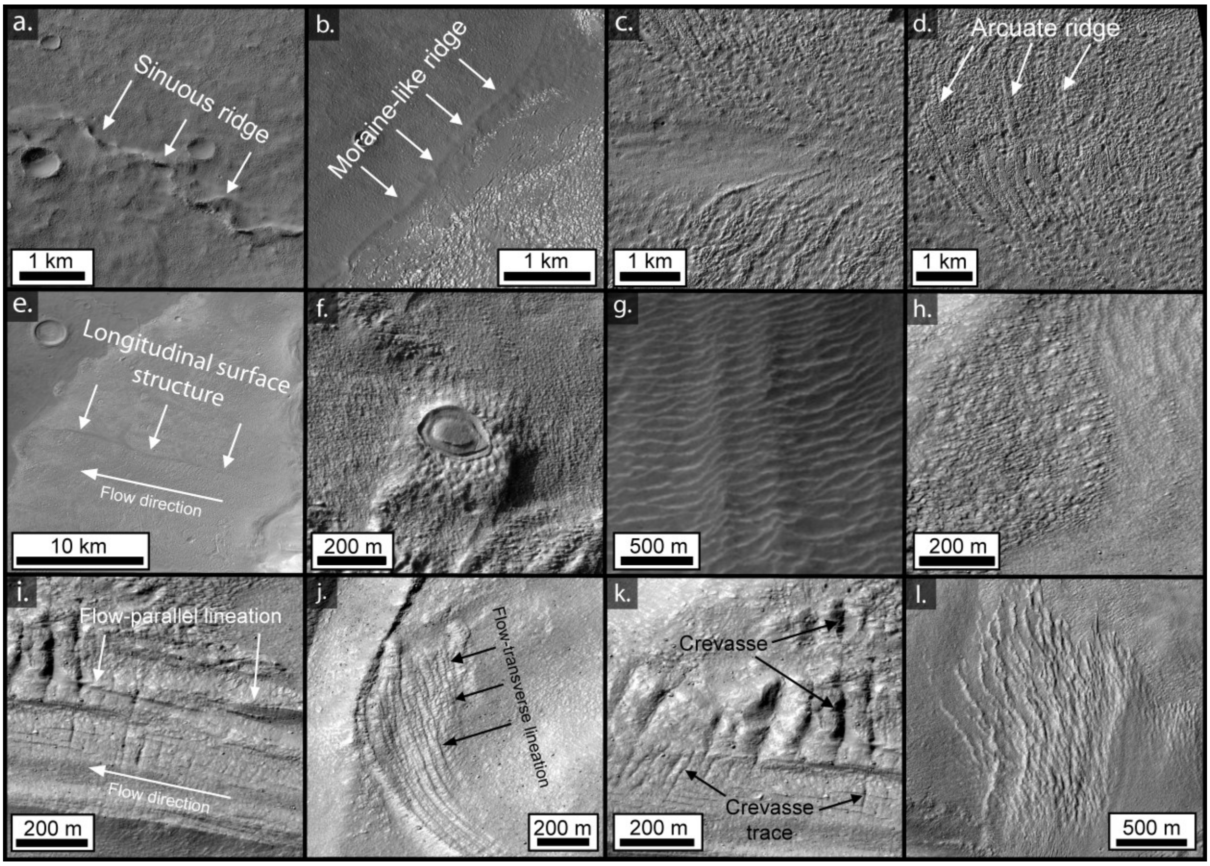
a.
Sinuous ridge
1 km
b.
Moraine-like ridge
1 km
c.
1 km
d.
Arcuate ridge
1 km
e.
Longitudinal surface structure
Flow direction
10 km
f.
200 m
g.
500 m
h.
200 m
i.
Flow-parallel lineation
Flow direction
200 m
j.
Flow-transverse lineation
200 m
k.
Crevasse
Crevasse trace
200 m
l.
500 m